catalysts

MDPI

Review

Catalysis-Based Cataluminescent and Conductometric Gas Sensors: Sensing Nanomaterials, Mechanism, Applications and Perspectives

Jinyun Liu [1,4,*], Tianli Han [2], Bai Sun [1], Lingtao Kong [1], Zhen Jin [1], Xingjiu Huang [1,3], Jinhuai Liu [1,3] and Fanli Meng [1,*]

1 Nanomaterials and Environmental Detection Laboratory, Institute of Intelligent Machines, Chinese Academy of Sciences, Hefei 230031, Anhui, China; bsun@iim.ac.cn (B.S.); ltkong@iim.ac.cn (L.K.); zjin@iim.ac.cn (Z.J.); xingjiuhuang@iim.ac.cn (X.H.); jhliu@iim.ac.cn (J.L.)
2 College of Chemistry and Material Engineering, Chaohu University, Chaohu 238000, Anhui, China; htl80@163.com
3 Department of Chemistry, University of Science and Technology of China, Hefei 230026, Anhui, China
4 Frederick Seitz Materials Research Laboratory, Beckman Institute for Advanced Science and Technology, University of Illinois at Urbana-Champaign, Urbana, IL 61801, USA
* Correspondence: jyliu@iim.ac.cn or jyliu@illinois.edu (J.L.); flmeng@iim.ac.cn (F.M); Tel.: +86-551-6559-1142 (J.L.); +86-551-6559-5607 (F.M.); Fax: +86-551-6559-2420 (J.L.)

Academic Editor: Keith Hohn
Received: 31 October 2016; Accepted: 13 December 2016; Published: 17 December 2016

Abstract: Gas environment detection has become more urgent and significant, for both industrial manufacturing and environment monitoring. Gas sensors based on a catalytically-sensing mechanism are one of the most important types of devices for gas detection, and have been of great interest during the past decades. However, even though many efforts have contributed to this area, some great challenges still remain, such as the development of sensitively and selectively sensing catalysts. In this review, two representative catalysis-based gas sensors, cataluminescent and conductometric sensors, the basis of optical and electric signal acquisition, respectively, are summarized comprehensively. The current challenges have been presented. Recent research progress on the working mechanism, sensing nanomaterials, and applications reported by our group and some other researchers have been discussed systematically. The future trends and prospects of the catalysis-based gas sensors have also been presented.

Keywords: catalysis; gas sensor; cataluminescence; conductometric measurement; nanomaterials; sensitivity

1. Introduction

Gas sensors based on a catalytically-sensing mechanism are one of the most important types of devices for gas environment detection. In the past decades, gas sensors have received broad attention due to their potential applications in industrial gas measurements, indoor air detection, coal gas monitoring, breath diagnosis, etc. [1–4]. Among the many catalysis-based gas sensors, cataluminescent and conductometric sensors, which rely on optical signal and current signal acquisition, respectively, are representative [5–8]. Sensing material is commonly the key part of the gas sensor. Therefore, the development of sensors mainly focuses on exploring high performance sensing materials during the past years.

Since Breysse et al. [9] first reported that the catalytic oxidation of carbon monoxide on the surface of thoria produced a chemiluminescent emission, and established the concept of cataluminescence, cataluminescence excited during the interaction between gases and catalyst surfaces has been

developed as a transduction principle for sensors. Cataluminescent gas sensors possess some significant advantages, such as stable and durable intensity, high signal/noise ratio, rapid response, and no consumption of analytes during detection [10,11]. However, until now, there are few practical applications of cataluminescent gas sensors, which is probably due to their unsatisfying sensitivity and selectivity, high requirement on the entire detection system, etc. Cataluminescence refers to a kind of chemiluminescence from the surface of solid catalysts during heterogeneous catalytic oxidation reactions. Generally, the cataluminescent reactions need the following factors: (i) suitable atmospheric environment containing oxygen such as the chemisorbed oxygen on the surface of catalysts; (ii) solid catalysts; and (iii) proper reaction temperature.

Conductometric sensors, on the basis of surface catalysis, similar to the cataluminescent sensors, are used to detect gases through acquiring the electric current of sensors with or without target gases. Semiconductor gas sensors are employed as typical conductometric sensors in this review. A large variety of semiconductors (e.g., ZnO, SnO_2, In_2O_3, WO_3, NiO, etc.) have been applied in gas sensors, which are widely used in portable gas detection systems because of their advantages including low cost, simple production, and compact size [12,13].

Until now, there have been some reviews about gas sensors [14–18]. However, there is a lack of a review particularly focused on the catalysis of cataluminescent and conductometric gas sensors, which is actually quite important for both basic scientific research and practical applications. Here, recent progresses on catalysis-based gas sensors including representative cataluminescent and conductometric sensors reported by our group and some other researchers are summarized comprehensively. The main challenges, working mechanism, sensing nanomaterials, applications and perspectives have also been discussed systematically.

2. Challenges for Catalysis-Based Gas Sensors

Depending on the development of hi-tech industrial manufacturing and the increasing demand of high quality gas environment in our daily life, gas detection based on sensors has become more significant, accompanied with a strict requirement for high sensing performance [19,20]. For example, as gas components are complicated, good selectivity is desired; in order to monitor gases at a trace concentration, ultra-high sensitivity with a low detection limit is necessary. To meet these requirements, catalysis-based gas sensors still have some great challenges:

(i) Developing small sized sensing materials is significant to achieve a high reactivity for catalytic reaction with target molecules. In recent years, nanomaterials have shown remarkably enhanced catalytic performance. Currently, a general preparation route that can apply extensive sensing nanomaterials is highly demanded.

(ii) Dealing with multi-component gases, two potential strategies could be considered: (a) improving the selectivity of gas sensor, which only shows response to a specific target gas; and (b) fabricating sensor array for multi-channel signal analysis simultaneously. The responding behaviors of different sensing materials toward different gases are not the same, making it possible to distinguish each target by combining with some algorithms such as principal component analysis (PCA) [21,22].

(iii) Acquiring weak sensing signals including cataluminescence and electric current is difficult when detecting trace concentration gases. In many cases, as the gas concentration reduces, sensing signal produced by sensors becomes poor [23,24]; thus, an efficient approach to acquire those signals and distinguish valuable data from noise is important for gas detection.

(iv) In order to reduce cost and simplify the operation procedures, a stable sensing performance of catalysis-based gas sensors is essential. However, commonly, high sensitivity would be in opposition to good long-term stability. Obtaining acceptable sensitivity and stability simultaneously remains a challenge. To achieve this, fabricating multi-functional structure and composite would be a potential strategy. For example, porous single-crystalline nanostructure is benefit for good gas adsorption, high reactivity, and structural stability.

(v) The catalytic mechanism of some sensing materials is not yet clear, which greatly restricts the design of novel high-performance sensing structures.

3. Cataluminescent Gas Sensors

3.1. Sensing Mechanism and Features

When oxygen molecules adsorb onto sensing material, the electron (e^-) in valence bond will be excited to conduction bond under a certain external energy stimuli, such as a heating treatment. At the same time, a cavity (h^+) forms in the valence bond, as shown in Figure 1. Such electron specie possesses a high capability of oxidization, which enables it to react with some target gas molecules represented as R. When gas molecules go through the surface of sensing materials, catalytic redox reaction happens, resulting in the formation of excited state intermediates. These intermediates go back to basic state, leading to the release of photon, and thus a chemiluminescence can be detected during this process. The chemiluminescence wavelength is determined by the energy structure and forbidden band of sensing materials [25,26]. The relative humidity in air is generally associated with the formation of chemisorbed hydroxyl groups, which may influence the surface catalysis during detection [27,28].

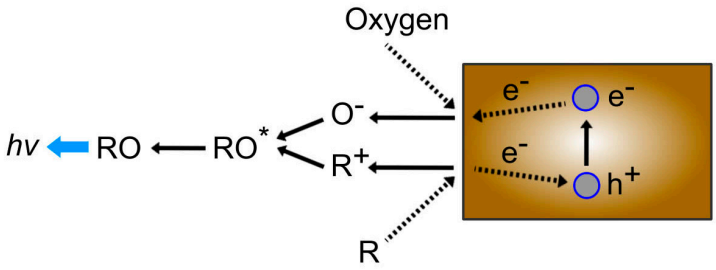

Figure 1. Sensing mechanism of cataluminescence-based gas sensor.

In recent years, nanomaterials and nanotechnologies have been developed rapidly, providing some new opportunities for fabricating high-performance cataluminescent gas sensors [29,30]. Thus, a series of cataluminescent gas sensors for specific applications can be designed on the basis of nanomaterials modulation. Those nanomaterials-based cataluminescent gas sensors would possess the following features: (i) External light resource is not necessary for gas detection. The influence factors to the sensing behaviors of cataluminescent gas sensors are reduced, which enhances the stability and accuracy. (ii) The luminescence is produced through the catalytic reactions on the interface between target gas and sensing nanomaterials, enabling a good reversibility. (iii) The selectivity of cataluminescent gas sensors can be significantly improved by specific modifications on sensing nanomaterials. (iv) Quantitative measurements are promising using the linear relationship of cataluminescent intensity versus gas concentration. Those attractive characteristics of cataluminescent gas sensors based on nanomaterials have attracted broad attention. Some recent research progresses on cataluminescent gas sensors for detecting different gases is presented below.

3.2. Typical Cataluminescent Detection System

Commonly, a cataluminescent detection system contains gas input unit, reaction unit and measurement unit. As illustrated in Figure 2, on the surface of a heating rod, a layer of cataluminescent materials is coated, which is then placed in a quartz tube. The working temperature can be modulated by controlling the voltage of the quartz tube. The pump controls the gas flow rate and disperses the target gas thoroughly. When the target gas flows through the tube, the catalytic reaction occurs on the surface of sensing materials. The cataluminescent intensity can be monitored by a photomultiplier tube equipped on a luminescence analyzer, which is commonly a Biophysics Chemiluminescence (BPCL) luminescence analyzer.

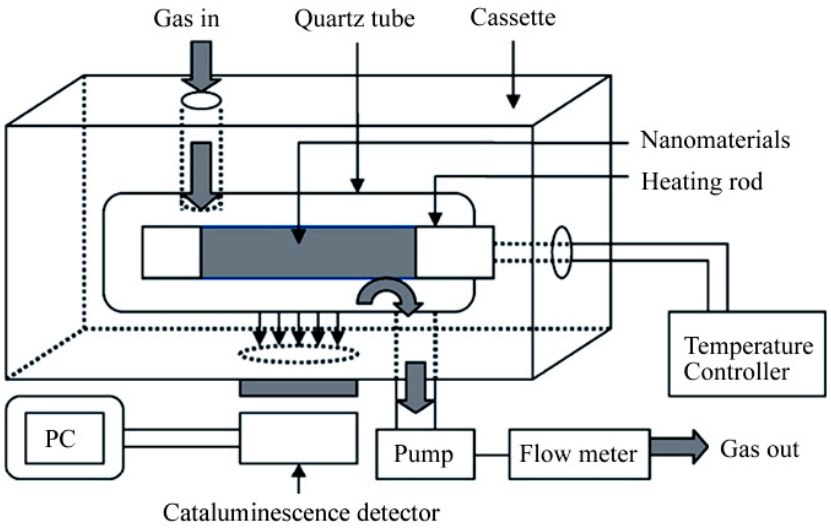

Figure 2. Illustration of a typical cataluminescent detection system, reproduced with permission from [31]. Copyright Elsevier, 2012.

3.3. Applications of Cataluminescent Gas Sensors

3.3.1. Cataluminescent Gas Sensors for Detecting Multi-Component Volatile Organic Compounds (VOCs)

VOCs generally exist in air, and they can cause short- or long-term adverse health effects [32]. Cataluminescent gas sensors have been demonstrated as highly efficient for VOC detection. Lv et al. [33] put forward a novel approach for the discrimination of gas compounds through a transient cataluminescence phenomenon on a flowerlike MgO. Using flowerlike MgO as sensing material, the cataluminescent gas sensor exhibits highly active, ultrafast, and characteristic responses toward many analytes, including isopropanol, methyl alcohol, tetrachloroethylene, ethyl alcohol, ethyl acetate, butanone, acetonitrile, methanoic acid, dichloromethane, epoxy chloropropane, etc., as shown in Figure 3. It is expected that for practical applications, it would be available to collect transient cataluminescence curves of multifarious compounds on different catalysts to establish a standard database, thus researchers could identify unknown samples by comparing their transient cataluminescence curves to standards. Zhang and co-workers showed a gas sensor for ketones detection based on cataluminescence generated on the surface of $NaYF_4$:Er nanomaterials [34]. When the Er^{3+} doping concentration is increased to 20%, the sensors show good sensing characteristics toward ketones. Under the optimal experimental conditions for detecting acetone and butanone, the gas sensor exhibits fast responses (3 s) and relatively low working temperature (250 °C). The linear ranges of cataluminescence intensity versus concentration are 2.388 to 143.28 $\mu g \cdot mL^{-1}$ for acetone and 2.45 to 49.0 $\mu g \cdot mL^{-1}$ for butanone, with a detection limit (signal-to-noise ratio = 3) of 1.7 and 0.7 $\mu g \cdot mL^{-1}$, respectively.

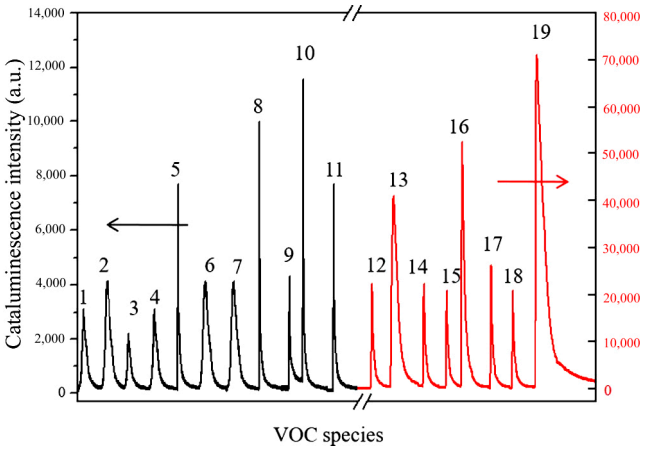

Figure 3. Typical responses of 19 kinds of volatile organic compounds (VOCs) on the MgO-based cataluminescent sensor: (**1**) isopropanol; (**2**) methyl alcohol; (**3**) tetrachloroethylene; (**4**) ethyl alcohol; (**5**) ethyl acetate; (**6**) butanone; (**7**) acetonitrile; (**8**) methanoic acid; (**9**) dichloromethane; (**10**) epoxy chloropropane; (**11**) carbon tetrachloride; (**12**) acetone; (**13**) isobutyl alcohol; (**14**) butanol; (**15**) butyraldehyde; (**16**) benzene; (**17**) propenoic acid; (**18**) butyl ether; and (**19**) diethyl ether. Working temperature, 220 °C; integral time, 0.5 s; VOCs concentration, 0.36 $\mu g \cdot mL^{-1}$, reproduced with permission from [33]. Copyright American Chemical Society, 2016.

Previously, we have reported cataluminescent gas sensors based on La_2O_3 and cocoon-like Au/La_2O_3 nanomaterials for detecting tetrahydrofuran, acetone, ethanol, benzene, chloroform and chlorobenzene [35]. $La(OH)_3$ precursors are firstly synthesized through a simple hydrothermal methods. After calcination at a high temperature, $La(OH)_3$ is converted to La_2O_3 on the basis of a dehydration reaction. The La_2O_3 shows a cocoon-like morphology after calcinations, as shown in Figure 4. In addition, Au/La_2O_3 is prepared by modifying Au nanoparticles onto $La(OH)_3$, which present a highly interconnected structure. It is advantageous for gas-sensing applications due to the high surface-to-volume ratio.

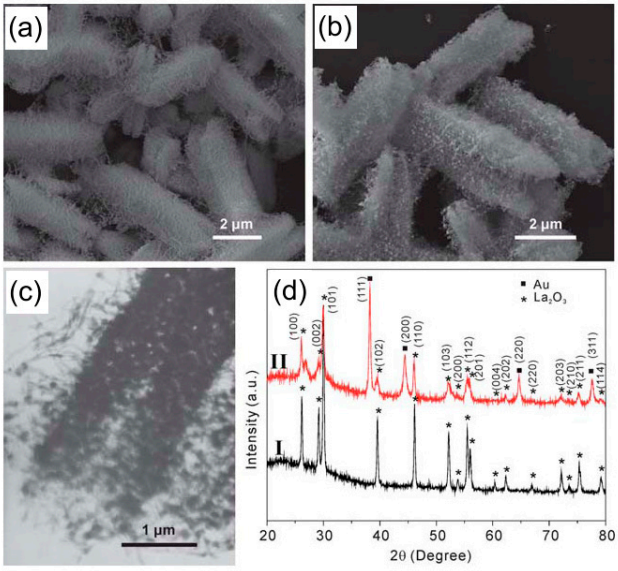

Figure 4. (**a**) Scanning electron microscopy (SEM) image of the cocoon-like La_2O_3; (**b**) SEM and (**c**) Transmission electron microscopy (TEM) images of Au/La_2O_3 nanomaterials; and (**d**) X-ray diffraction (XRD) patterns of the La_2O_3 and Au/La_2O_3 nanostructures, reproduced with permission from [35]. Copyright Royal Society of Chemistry, 2011.

The cocoon-like Au/La_2O_3-based sensors exhibit high responses to VOCs compared to the unmodified sensor under the same working conditions, as shown in Figure 5. The pristine La_2O_3 sensors show weak responses to tetrahydrofuran, acetone, and ethanol, while there is no response to benzene, chloroform, and chlorobenzene. After functionalization with Au nanoparticles, the cataluminescence intensities are evidently enhanced. The relative intensities go up to ca. 2179, 1808, 733, 2395, 458 and 270 to tetrahydrofuran, acetone, ethanol, benzene, chloroform and chlorobenzene, respectively. In addition, the response/recovery times are quite short. The high cataluminescent performance might be ascribed to the functional Au nanoparticles, which provide extraordinary catalysis activity. Oxygen species dissociating from Au nanoparticles, which possess high catalytic abilities, would migrate to the surface of La_2O_3, resulting in the increase of oxygen species concentration [36], which is significant for achieving a high catalytic activity in terms of the cataluminescent mechanism. The Au/La_2O_3-based cataluminescent gas sensors present good cataluminescence performance such as high intensity and signal/noise ratio, and fast response/recovery to targets, making them can be promisingly applied for the detection of VOCs in environment.

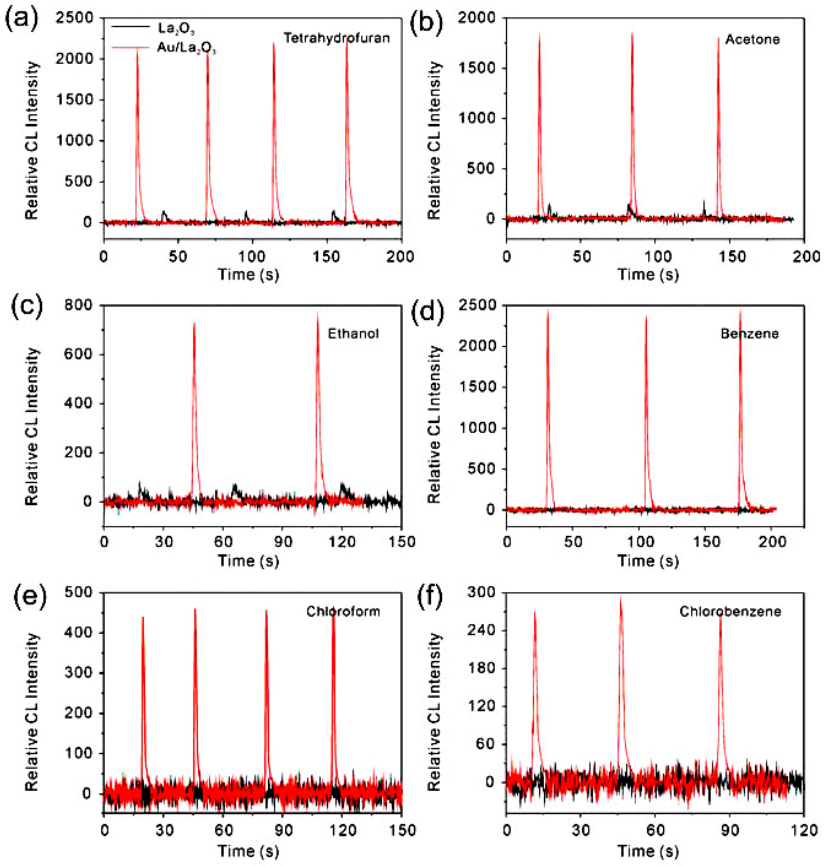

Figure 5. Cataluminescent responses of the cocoon-like Au/La_2O_3 and La_2O_3-based sensors to different VOCs (200 ppm) at 300 °C: (**a**) tetrahydrofuran; (**b**) acetone; (**c**) ethanol; (**d**) benzene; (**e**) chloroform; and (**f**) chlorobenzene, reproduced with permission from [35]. Copyright Royal Society of Chemistry, 2011.

Even though the cataluminescent responses shown above are quite attractive, the selectivity and recognition of specific target gases still remain a challenge. With this in mind, some studies focus on the modification of sensing materials [37,38]. Conversely, we have demonstrated a sensor array strategy for effective recognition of different gases. Twelve VOCs have been discriminated based on a cataluminescent patterns obtained by a 4 × 4 nanomaterial-based array (Figure 6) [39]. The airflow is supplied by a pneumatic pump and a precision flow meter is employed for the measurement of

the gas flow rate. A digital temperature controller is used to control the temperature of the ceramic chip. The final cataluminescent patterns are recorded by a camera closely placed to the ceramic chip after inputting target gas for about 1 min. The results indicate that the patterns with a relatively weak brightness of spots for chloroform and toluene can be obtained at 190 °C, as shown in Figure 7. When the temperature is increased to 210 °C and 230 °C, the brightness of the spots is feasible to differentiate ether, acetone, chloroform, and toluene. This finding indicates different patterns can be obtained at different working temperature, whichcan distinguish each VOC gas.

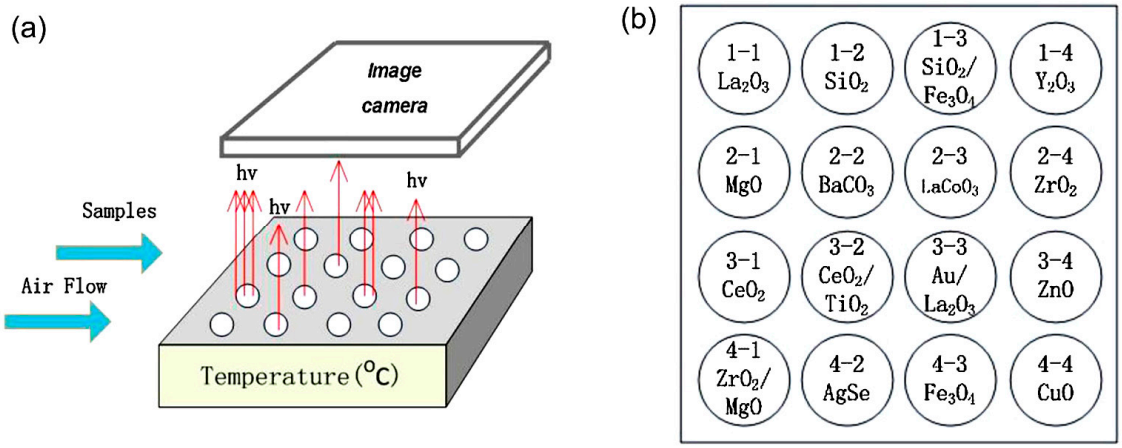

Figure 6. (**a**) Schematic diagram of the cataluminescent sensor array; and (**b**) arrangement of nanomaterials spots, reproduced with permission from [39]. Copyright Elsevier, 2013.

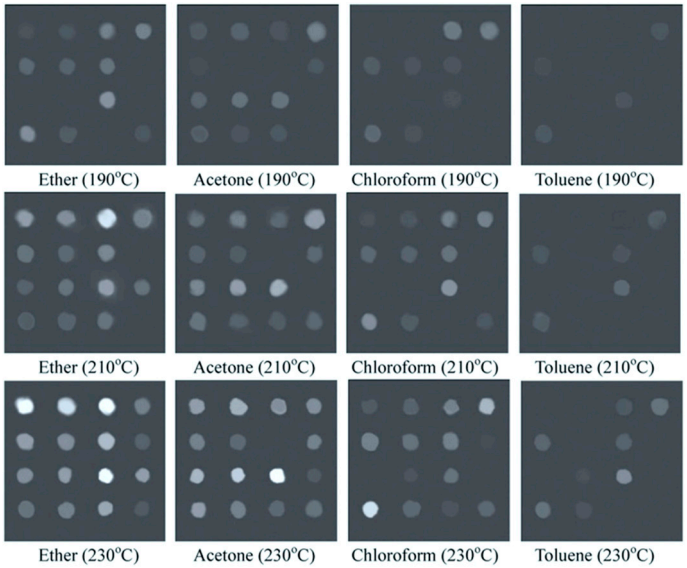

Figure 7. The patterns of the sensor array at different working temperatures. The concentrations of the VOCs: 2000 ppm; flow rate of carrier gas: 240 mL·min^{-1}, reproduced with permission from [39]. Copyright Elsevier, 2013.

3.3.2. Cataluminescent Gas Sensors for Detecting Alcohol

Zhang and co-workers have fabricated a cataluminescent gas sensor for alcohol detection on the basis of the chemiluminiscence characteristics between $SrCO_3$ nanomaterials and alcohol [40]. They have investigated the influences of temperature and gas flow rate to sensing performance. The sensing range is around 6 to 3750 ppm. The detection limit is as low as 2.1 ppm. Moreover, they demonstrated that the $SrCO_3$-based chemiluminiscent gas sensor exhibited a selectivity to alcohol

with no response to gasoline, ammonia, or hydrogen. Such a specific gas sensor can be potentially applied for breath diagnosis and industrial gas monitoring.

However, those gas sensors still demand a high working temperature to activate cataluminescent reactions. For example, a temperature of about 470 °C is needed for detecting alcohol using a TiO_2-based cataluminescent sensor. Such a high temperature would induce a strong luminescence basis, which reduces the signal/noise ratio severely. Moreover, high temperature consumes energy, which is disadvantage for portable instrument since the power of batteries is limited. Therefore, a low temperature cataluminescent gas sensor is highly required. Zhang et al. [41] reported that ZrO_2 nanomaterials exhibited a good cataluminescent property at a relatively low temperature of 195 °C. The fabricated sensor shows a high stability even after working for 100 h. At a wavelength of 460 ± 10 nm, the ZrO_2 cataluminescence sensor exhibits a detection limit of 0.6 ppm to alcohol, while the detecting linear range is from 1.6 to 160 ppm.

Zhang et al. have also figured out a cataluminescent mechanism on the basis of energy transfer [42]. Once some metal ions such as Ho^{3+}, Co^{2+}, and Cu^{2+} are introduced into sensing materials, cataluminescent would be quenched. Meanwhile, the active intermediates formed during catalytic reactions transfer to those doping ions. On the basis of this finding, they reported a Eu-doped ZrO_2 cataluminescent gas sensor, which shows a high sensing performance for alcohol detection. The sensitivity of Eu-doped ZrO_2 sensor is about 72 times the ZrO_2 sensor without doping. They demonstrated that such a great performance enhancement could be explained as follows: when alcohol molecules react with ZrO_2, some of the active intermediates are absorbed by catalyst ZrO_2; once there are Eu^{3+} dopants in the sensing nanomaterial, active intermediates would transfer to Eu^{3+}, resulting in the improvement of sensitivity. Their findings also indicate that the main factor limiting the sensitivity of cataluminescent gas sensor based on pure catalyst may be the inevitable energy quenching of excited intermediates with the catalyst. This point has also been confirmed by Lu et al. [43]. They indicated that the chemisorbed oxygen on the surface of catalysts was one of the essential factors for catalytic oxidization of gaseous molecules during the cataluminescent process.

In addition, Zhang's research group prepared a TiO_2 nanomaterial with a particle size of about 20 nm through a sol-gel route [44]. They found that TiO_2 nanoparticles exhibit strong cataluminescent intensity once they react with alcohol and acetone. Their results show that the linear relationships are good in the concentration ranges of 40 to 400 ppm for alcohol and 20 to 200 ppm for acetone. Lv and co-workers reported ZnO nanoparticles could react with alcohol and produce luminescence [45]. They fabricated a ZnO-based cataluminescent gas sensor for detecting alcohol. A good linear relationship between cataluminescent intensity and alcohol vapor concentration is obtained in the range of 1 to 100 ppm, while the detection limit is about 0.7 ppm.

3.3.3. Cataluminescent Gas Sensors for Benzene Detection

Benzene is a colorless and volatile liquid with a strong aroma. Benzene vapors released from building materials and some plastic applications used in our daily life can rise up the risk of many diseases to human. Monitoring benzene with cataluminescent gas sensors have been of great interest. It was reported that cataluminescent sensors showed a good linear relationship (Figure 8a) and a selectivity towards benzene from some gas interferences (Figure 8b), including propanol, butanol, formaldehyde, butanone, dimethylbenzene, methanol, and toluene under the same conditions at a concentration of about 800 ppm [46]. There is no signal for propanol, dimethylbenzene and methanol, while the intensity to benzene is particularly high. Zhang et al. [47] have confirmed that the selectivity, sensitivity and lifetime of the cataluminescent sensors are greatly dependent on the following factors: the careful selection of cataluminescent reagents responding to the definite species, the method of immobilizing the reagents, and the substrates selected for reagents immobilization.

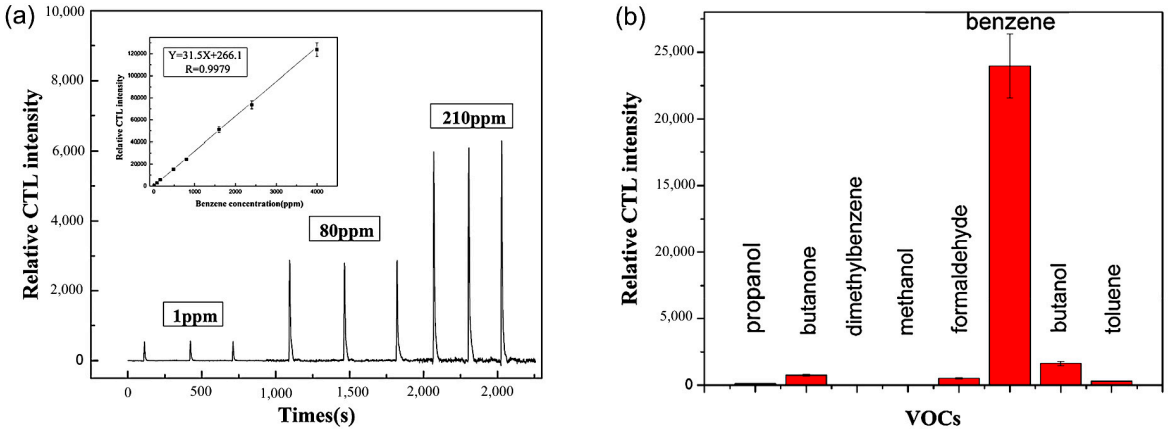

Figure 8. (**a**) Sensing curves of the cataluminescent sensor to benzene at different concentrations ranging from 1 to 210 ppm. The inset shows the linear relationship between cataluminescence and gas concentration. (**b**) The selectivity towards benzene from gas interferences. Flow rate of carrier gas: 200 mL·min^{-1}; temperature of sensor: 210 °C; gas concentration: 800 ppm; wavelength: 420 nm, reproduced with permission from [46]. Copyright John Wiley & Sons, 2013.

3.3.4. Cataluminescent Gas Sensors for Ether Detection

The low-cost and portable approach for ether detection is required because of the increasing attention on environmental monitoring, homeland security, agriculture, and medical applications [48–50]. Ether is widely used both in laboratory and industry. However, continued exposure to ether may lead to respiratory failure or even death due to its anesthetic effect [51]. Cataluminescent gas sensors have been developed for sensitive ether detection in the past few years. For example, Li et al. [31] synthesized some SiO_2/Fe_3O_4 microspheres which showed a high cataluminescent performance toward ether, as shown in Figure 9. The results indicate that the SiO_2/Fe_3O_4 microsphere-based sensors exhibit good cataluminescent properties including stable intensity, high signal/noise values, short response and recovery time. After optimization, the gas sensor possesses a linear detection range from 10 to 3000 ppm (r = 0.9967) and a detection limit of about 6.7 ppm (S/N = 3), which is much below the standard permitted concentration of ether in indoor air.

Lu and co-workers used mesoporous TiO_2 nanoparticles to detect diethyl ether with a 440 nm bandpass filter. The cataluminescent gas sensor shows high selectivity toward diethyl ether over other VOCs, such as acetaldehyde, acetone, butanone and butanol, etc. The selectivity is ascribed to the difference of cataluminescent emission profiles of various VOCs reaction intermediates. They confirmed that only diethyl ether exhibited a strong cataluminescent emission at about 440 nm. Wang et al. [52] reported a three-dimensional hierarchical CdO nanostructure with a bio-inspired morphology which showed outstanding cataluminescent properties such as stable intensity, high signal/noise values, short response and recovery time. The limits of detection toward acetone and diethyl ether are ca. 6.5 and 6.7 ppm, respectively. In addition, a principal components analysis method was demonstrated to be able to recognize acetone and diethyl ether clearly.

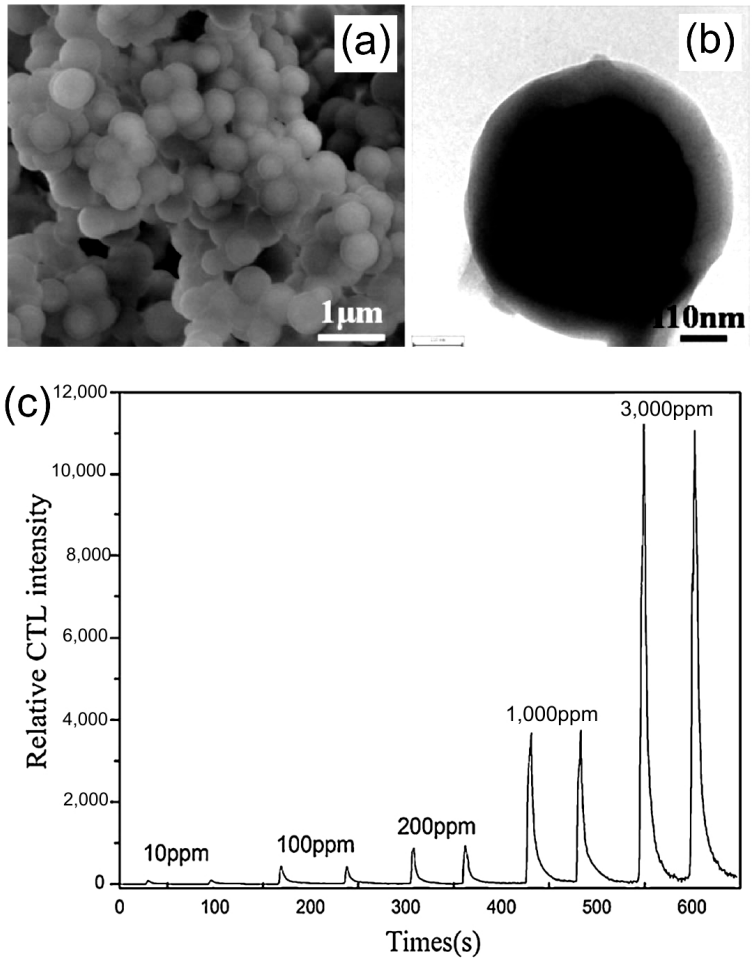

Figure 9. (**a**) SEM and (**b**) TEM images of the SiO_2/Fe_3O_4 microspheres; and (**c**) cataluminescent curves of the SiO_2/Fe_3O_4-based gas sensor. Flow rate: 240 mL·min^{-1}; temperature of sensor: 310 °C; wavelength: 431 nm, reproduced with permission from [31]. Copyright Elsevier, 2012.

3.3.5. Cataluminescent Gas Sensors for Detecting Aldehyde

$BaCO_3$ nanomaterials were reported to have a good cataluminescent response to acetaldehyde [53]. $BaCO_3$-based gas sensor gives high sensitivity and selectivity to acetaldehyde at a working temperature of about 225 °C. At a wavelength of 555 nm, the linear range of cataluminescent intensity versus concentration of acetaldehyde is 2 to 2000 ppm, with a detection limit of 0.5 ppm (signal-to-noise ratio = 3). Ignorable levels of interference are observed while cyclohexane, *n*-hexane, carbon tetrachloride, ammonia, methylbenzene, chloroform, benzene, formaldehyde, ethanol and carbon dioxide are passing through the cataluminescent gas sensor.

For acetaldehyde detection, a zeolite-based cataluminescence gas sensor was reported by Liu et al. [54]. They found that the reactions between acetaldehyde and O atoms in the cages of large-pore zeolites could result in a light emission. The zeolite-based cataluminescence sensor shows a linear response from 0.06 to 31.2 ppm toward acetaldehyde vapor. In addition, methanol, ethanol, isopropanol, methylbenzene, chloroform, dichlormethane and acetonitrile do not impact the cetaldehyde determination on CsNaY catalyst. More interesting, acetaldehyde vapor could be distinguished from some homologous series, including formaldehyde, cinnamaldehyde, glutaraldehyde and benzaldehyde. They considered that the mechanism could be due to the stereoselectivity of zeolite.

A sensitive cataluminescence-based gas sensor for the determination of formaldehyde using nanosized $V_2Ti_4O_{13}$ as a probe has been reported by Zhou et al. [55]. The sensor exhibits a high

selectivity to formaldehyde at 490 nm and a good activity at 370 °C. The linear range is 0.1 to 40 ppm (r = 0.9995), and the detection limit is as low as 0.06 ppm. In addition, the sensor is applied for detecting formaldehyde in artificial gas, showing rapid response, high selectivity, and long lifetime for practical environmental analysis.

3.3.6. Cataluminescent Gas Sensors for Detecting Inorganic Gas H_2S

Previously, a Fe_2O_3-based cataluminescent gas sensor was reported for H_2S detection [56]. When H_2S gas passes through the surface of Fe_2O_3 catalyst, it is catalytically oxidized to SO_2 by oxygen in air. Electronically excited SO_2 molecules are produced during the reaction, and the cataluminescence is generated when they return to basic state. On the basis of this mechanism, the Fe_2O_3-based cataluminescent gas sensor shows a high selectivity to H_2S without response to 12 other kinds of gases such as hydrocarbon, alcohol, NO_2, and so on. The response time is within 15 s while the recovery time is less than 120 s. The linear range of the sensor is in the range from 8 to 2000 ppm with a detection limit of 3 ppm.

Zhou et al. [57] reported a cataluminescent sensor for simultaneous detection of formaldehyde and H_2S in air. The cataluminescence is emitted from the surface of $Zn_3SnLa_2O_8$ nanomaterials operating at a temperature of 275 °C. The limits of detection are 0.07 ppm for formaldehyde and 0.22 ppm for H_2S, respectively. Furthermore, they found that some potential interferences, such as vapors of acetaldehyde, ethanol, benzene, toluene, ethylbenzene, ammonia, sulfur dioxide, carbon dioxide, nitric oxide and nitrogen dioxide, did not disturb the performance of the $Zn_3SnLa_2O_8$ sensor.

Recently, lv's group [6] reported a metal-organic frameworks (MOFs)-based cataluminescent sensor. Four MOFs, MIL-100(Fe), MIL-101(Cr), $Zn_3(BTC)_2{\cdot}12H_2O$ and ZIF-8, are investigated as cataluminescence sensing materials. Among them, MIL-100(Fe) shows high cataluminescence intensity for H_2S. This group also prepared α-Fe_2O_3/g-C_3N_4 composites for cataluminescence sensing of H_2S [58]. They found when the α-Fe_2O_3 in the composite reached 5.97%, the cataluminescence responses became high. The linear detection range is 0.88 to 7.01 $\mu g{\cdot}mL^{-1}$ (r = 0.998) with a detection limit of 0.5 $\mu g{\cdot}mL^{-1}$ (S/N = 3). In addition, the cataluminescence gas sensor exhibits a good selectivity to H_2S compared to other fourteen VOCs with a fast response (0.1 s) and recovery (0.6 s), showing a promising application for practical monitoring H_2S gas.

For the catalyst-based sensors indicated above, a brief summary about their gas-sensing performance is shown in Table 1.

Table 1. The comparison on the sensing performance of gas sensors based on different catalysts.

Cataluminescent Sensing Catalysts	Target Gases	Limit of Detection	Linear Range of Cataluminescence Intensity vs. Concentration	Reference
Nanosized $NaYF_4$:Er	acetone and butanone	1.7 μg·mL^{-1} for acetone; 0.7 μg·mL^{-1} for butanone	2.388–143.28 μg·mL^{-1} for acetone; 2.45–49.0 μg·mL^{-1} for butanone	[34]
Nanosized $SrCO_3$	ethanol	2.1 ppm	6–3750 ppm	[40]
Nanosized ZrO_2	ethanol	0.6 μg·mL^{-1}	1.6–160 μg·mL^{-1}	[41]
Eu^{3+}-doped nanosized ZrO_2	ethanol	15 ppm	45–550 ppm	[42]
Y_2O_3	ethyl ether	0.5 mM	1.0−100 mM	[43]
TiO_2	ethanol and acetone	10.5 μg·mL^{-1} for ethanol; 6.7 μg·mL^{-1} for acetone	40–400 μg·mL^{-1} for ethanol and 20–200 μg·mL^{-1} for acetone	[44]
ZnO nanoparticles	ethanol	0.7 ppm	1.0–100 ppm	[45]
Au/La_2O_3 nanomaterials	benzene	0.7 ppm	1–4000 ppm	[46]
SiO_2/Fe_3O_4 microspheres	ether	6.7 ppm	10–3000 ppm	[31]
CdO nanostructure	acetone and diethyl ether	6.5 ppm for acetone; and 6.7 ppm for diethyl ether	8–3000 ppm for acetone; and 10–4000 ppm for diethyl ether	[52]
Zeolite	Acetaldehyde	0.02 μg·mL^{-1}	0.06–31.2 μg·mL^{-1}	[54]
Nanosized $V_2Ti_4O_{13}$	formaldehyde	0.06 mg·m^{-3}	0.1–40 mg·m^{-3}	[55]
Fe_2O_3	H_2S	3 ppm	8–2000 ppm	[56]
Nanosized $Zn_3SnLa_2O_8$	formaldehyde and H_2S	0.07 mg·m^{-3} for formaldehyde; and 0.22 mg·m^{-3} for H_2S	0.2–61.7 mg·m^{-3} for formaldehyde; and 0.4–68.5 mg·m^{-3} for H_2S	[57]
Metal-organic frameworks	H_2S	4.4 ppm	100–300 mL·min^{-1}	[6]

4. Catalysis-Based Conductometric Semiconductor Gas Sensors

4.1. Sensing Mechanism and Features

According to carrier type such as electron or cavity, semiconductor gas sensors can be classified into *n*-type (e.g., CdO and SnO_2) and *p*-type (e.g., NiO) sensors [59,60]. Most gas sensors are *n*-type, in which electrons are carriers instead of cavities during sensing process. The introduction of the catalytically sensing mechanism given below is on the basis of *n*-type metal oxides sensors. Although the exact fundamental mechanism is still controversial, it is commonly accepted that the conductometric changes of the semiconductor gas sensors are caused by the surface catalysis reaction between metal oxides and gas molecules [61,62].

For the *n*-type semiconductor gas sensor, the sensing process is that oxygen gases are adsorbed on the surface of semiconductor in air. The adsorbed oxygen species capture electrons from the inner of semiconductor. The negative charges trapped in these oxygen species cause a carrier depletion layer and thus reduce the conductivity. When the sensor is exposed to reducing gases, gas molecules will be oxidized by the active oxygen species while the electrons trapped by the active oxygen species return to semiconductor, leading to a decrease of the potential barrier height and an increase of conductivity. There are different active oxygen species including molecular (O_2^-) and atomic (O^-, O^{2-}) ions on the surface of semiconductors depending on the working temperature. Generally, the molecular form is dominant below 150 °C, while the atomic oxygen species are found above this temperature [63,64].

4.2. Conductometric Detection System

Generally, there are two types of conductometric sensor structures: directly heated sensors and indirectly heated ones. A directly heated sensor means that the heater contacts with the sensing materials, which might lack stability and add anti-interference ability. Thus, most current nanostructure-based gas sensors are indirectly heated sensors, which can be further divided into two device structures, i.e., cylindrical and planar layouts (Figure 10). Alumina ceramics (wafers or tubes) are generally used as substrates to support sensing films. In the ceramic tube-based sensors, a heating wire is placed inside the ceramic tube, while in the ceramic wafer-based sensors, a layer of heating paste is on the backside of ceramic wafer. Some silica wafers can also be used as the substrate, which is advantageous for manufacturing small sized gas sensors because of its compatibility with integrated circuits.

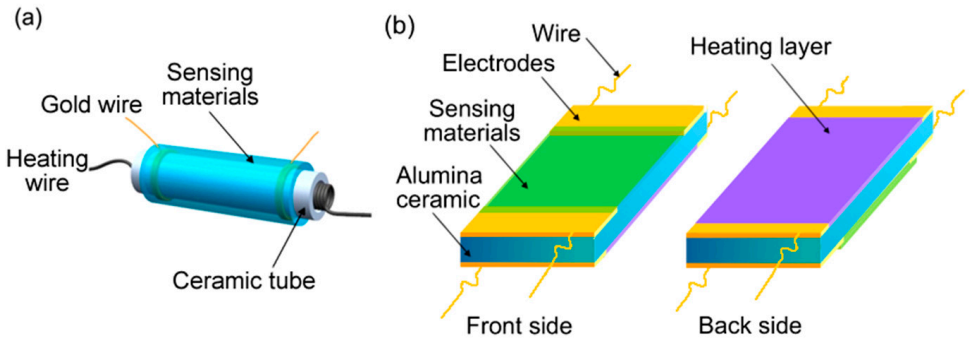

Figure 10. (**a**) Cylindrical; and (**b**) planar structures of catalysis-based conductometric gas sensors.

Gas-sensing measurement is usually conducted within a closed chamber with a volume of about 1000 mL equipped with appropriate gas flow inlet and outlet, as shown in Figure 11. During a typical gas-sensing detection, a constant voltage is applied onto the pair of electrodes between sensing films, then the current is measured and recorded by an amperemeter connected with a computer. A certain concentration of target gas in air is introduced into the test chamber, while after measurement the

target gas is released by inputting fresh air. The acquired current signal is used for further gas-sensing performance analysis.

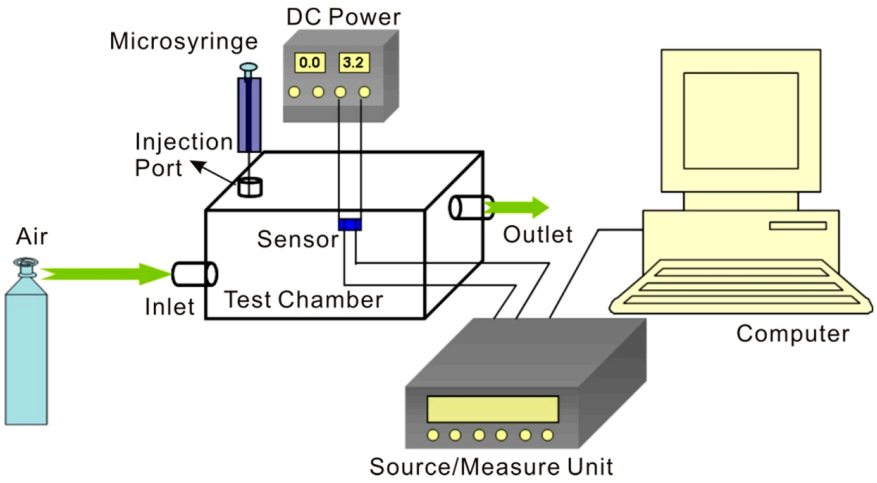

Figure 11. Schematic diagram of the conductometric detection system.

4.3. Applications of Catalysis-Based Conductometric Semiconductor Gas Sensors

Although semiconductor gas sensors have been widely used in portable gas detection systems, the sensing performance is significantly influenced by the morphology and structure of sensing materials, resulting in a great obstacle for gas sensors based on bulk materials or dense films to achieve highly-sensitive properties [65–67]. Conductometric gas sensors based on nanomaterials are promising to improve gas-sensing properties including sensitivity, selectivity and response/recovery speeds due to their large specific surface area and high catalysis activity [68–70]. Here, some nanomaterial-based semiconductor gas sensors are summarized to show the gas-sensing enhancement effect. Different from the classification method of previous cataluminescent gas sensors by following the target gases, conductometric sensors are introduced on the basis of different types of sensing materials.

4.3.1. Noble Metal Nanoparticle Enhanced Catalytically Sensing Effect

Noble metal nanoparticles commonly possess high catalysis properties. They have been used widely to modify metal oxide semiconductors to enhance the gas-sensing performance [71,72]. Up to now, significant efforts have been made to improve the sensitivity and selectivity to VOCs by doping noble metals in metal oxides [73]. As one of the most popular sensing metal oxides, ZnO has been investigated in the past decades because of its excellent electronic and optical properties [74,75]. Various ZnO nanostructures such as nanowires [76–78], nanorods [79,80], nanosheets [81] and nanospheres [82] have been developed. In particular, porous single-crystalline ZnO nanosheets have been synthesized, which not only exhibit highly sensitive performance but also possess significantly long-term stability. Therefore, surface modification of noble metals on those porous single-crystalline ZnO nanosheets would be promising. We have reported Ag nanoparticles-modified ultra-thin porous single-crystalline ZnO nanosheets, which exhibit high sensitivity to ethanol with a detection limit of 1 ppb [83,84]. Similarly, Pt nanoparticles are decorated to porous single-crystalline ZnO nanosheets, which show good response to low concentrations of chlorobenzene from 10 to 500 ppb [85].

Hierarchical structures may provide more spaces for gas diffusion into the deep place of the sensing film [86–88]. For example, Mohammad et al. [89] prepared a hierarchical structure based on ZnO nanowire or nanodisk which possessed high surface area to volume ratio and an increased proportion of exposed active planes. Those hierarchical ZnO structures showed significantly improved sensitivity and fast response to acetone compared to some other mono-morphological ZnO. Therefore, assembling the porous single-crystalline ZnO nanosheets into flower-like hierarchical structures may further improve the sensing properties because three-dimension (3D) hierarchical structures can provide more spaces for gas diffusion [90,91]. Thus, Au nanoparticles are used to modify flower-like hierarchical ZnO structures assembled by porous single-crystalline nanosheets, which is super-sensitive to acetone with a detection limit of 0.5 ppb [92]. Pt nanoparticles are also modified onto the surfaces of In_2O_3 hierarchical structures, which could exhibit excellent responses to CO at room temperature [93].

Primarily, there are two sensitization mechanisms generally considered for noble metal modification, i.e., the electronic sensitization caused by interfacial electronic redistribution and the chemical sensitization caused by interfacial atom transport [94]. In the electronic sensitization mechanism, electrons are extracted from the oxide (ZnO) to the noble metal nanoparticles due to the work function difference and enriched there, which results in an increase in the depth of the electron depletion layer in the oxide. Because the potential barrier height between neighboring grains is elevated, the noble metal decorated oxide sensor will become more sensitive to the change in environmental atmosphere. Ag nanoparticles are mostly considered to function as electronic sensitization mechanism. However, Au and Pt nanoparticles mostly enhance the sensing performance through its catalytic activity by a chemical sensitization mechanism, which is also known as the spillover effect and has been well-established in the catalysis process of metal-supported catalysts. In this mechanism, the noble metal may provide more active sites for the adsorption of molecular oxygen and target gases and facilitate the dissociation of these molecules due to their highly catalytic or conductive nature. In air, the oxygen anions adsorbed on noble metals will diffuse into the surface region of oxides near the noble metals. In the sensing process, the target gases are activated by the noble metals as well, and then spill over and are oxidized by the adsorbed oxygen anions near the noble metals.

Jang et al. have reported vertically ordered SnO_2 nanorods decorated with Au nanoparticles, which could detect sub-ppb levels of volatile reducing gases with a fast response speed due to the sensitization effects of the Au nanoparticles, as shown in Figure 12 [95]. It has been confirmed that Au nanoparticles residing in the bamboo joint-like spaces enabled the SnO_2 nanobamboos to detect sub-ppb level of target gases by maximizing the enhancement of the depletion region. In addition, they reported a facile method for the utilization of metal decoration on both the inner and outer surfaces of hollow metal oxide nanostructure. Close-packed SnO_2 nanodome arrays decorated with Au nanoparticles are fabricated by soft-template method and self-agglomeration of an Au film [96]. The Au-decorated sensor shows a response 18 times higher than that of the bare SnO_2 nanodome arrays to C_2H_5OH at 300 °C. Through the general method, some other noble metals such as Pd and Ag can also be decorated onto sensing materials which exhibit much enhanced gas-sensing performance [97,98].

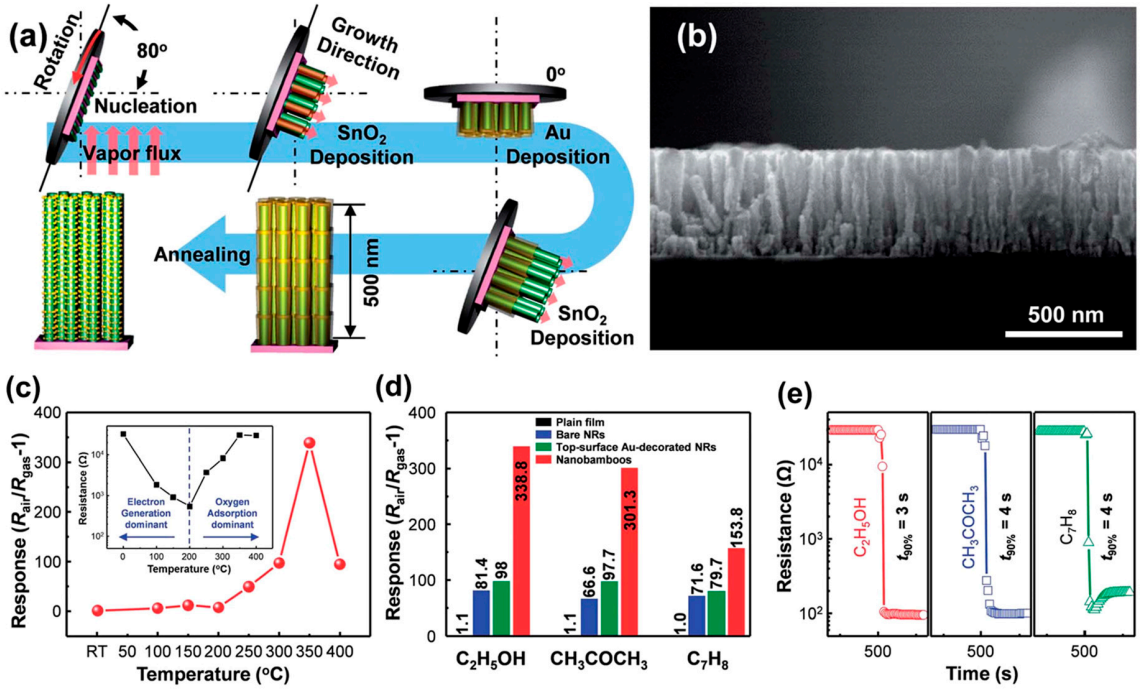

Figure 12. (**a**) Schematics of the fabrication procedures of the SnO_2 nanobamboos; (**b**) cross-sectional SEM image of the SnO_2 nanobamboos; (**c**) responses of the SnO_2 nanobamboos to 50 ppm of C_2H_5OH at different operating temperatures (inset in (**c**) shows the baseline resistance of the SnO_2 nanobamboos as a function of temperature in air); (**d**) responses to 50 ppm C_2H_5OH, CH_3COCH_3, and C_7H_8 for plain SnO_2 films, bare SnO_2 nanorods, top-surface Au-decorated SnO_2, and SnO_2 nanobamboos at optimal temperature; and (**e**) response curves and 90% response times of the SnO_2 nanobamboos to 50 ppm C_2H_5OH, CH_3COCH_3, and C_7H_8, reproduced with permission from [95]. Copyright Royal Society of Chemistry, 2015.

4.3.2. Small Size Effect on Catalysis-Based Conductometric Gas Sensors

The small size effect of metal oxides refers to the effect that when the particle size decreases the sensitivity of the sensor increase. Xu et al. have explained the phenomena by a semiquantitative model [99]. Three different cases can be distinguished according to the relationship between particle size (D) and the width of depletion layer (L) which is produced around the surface of crystallites. When the particle size is less than double of the width of its depletion layer, the sensor becomes highly sensitive to ambient gas molecules. However, small sized nanoparticles are inclined to aggregate because of their high surface energy.

To resolve this issue, SnO_2/graphene nanocomposites were prepared by a wet chemical method [100]. The formation process of SnO_2/graphene nanocomposites is illustrated in Figure 13. There are many functional groups on graphene including hydroxyl and epoxy groups on the planes, as well as carboxyl groups at the edges, which acts as anchor sites to enable stannic ions attaching onto the graphene [101,102]. Since graphene are two-dimensional, the size of SnO_2 colloids can be quite small on the basis of the steric hindrance effect [103]. The SnO_2/graphene nanocomposites exhibit an improved sensitivity compared to traditional SnO_2. Trace benzene is detected using the SnO_2/graphene. The detection limit is as low as 5 ppb. Besides, owing to the π-conjugate with graphene, the responses to benzene are higher than to ethanol. Similar findings are also confirmed for the SnO_2/MWCNT nanocomposites, which are highly sensitive to persistent organic pollutants (POPs) [104]. According to the report, the gas sensing properties of SnO_2/graphene nanocomposites are better than that of SnO_2/MWCNT nanocomposites because that graphene could make more abundant exposure of the sheet surface to the environment [103].

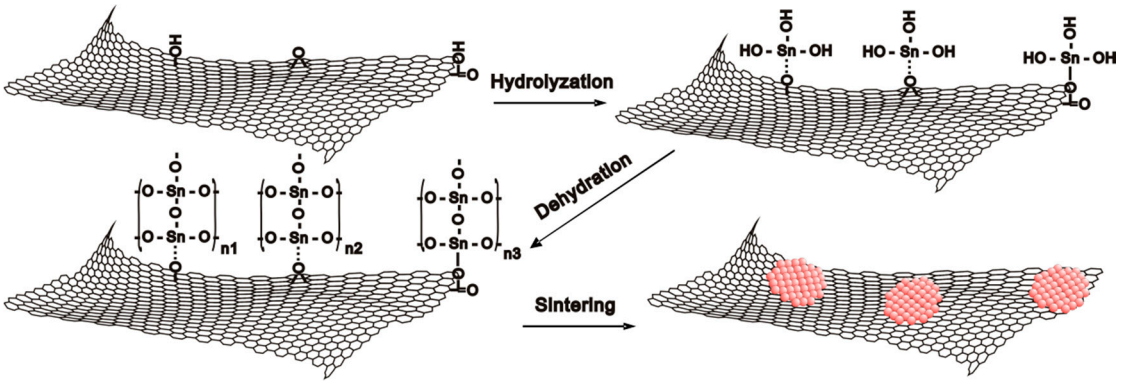

Figure 13. Illustration for the formation mechanism of the SnO_2/graphene nanocomposites, reproduced with permission from [93]. Copyright Elsevier, 2012.

4.3.3. Combination of the Catalytic Effects of Noble Metal Nanoparticles and Small Size

Graphene has been used to prepare nanocomposite with SnO_2 previously, in which the SnO_2 nanoparticles are uniform, small and well dispersed [105]. It is found that by combining with the π-conjugate function of graphene, the SnO_2/graphene nanocomposites exhibit a highly sensitive performance to benzene. However, the SnO_2/graphene shows low sensitivity to other VOCs. For some specific applications, noble metal is modified onto the SnO_2/graphene nanocomposites. It was reported that Ag/SnO_2/Graphene ternary nanocomposites were sensitive to acetone [106]. Figure 14 shows the response comparison between Ag/SnO_2/graphene and SnO_2/graphene nanocomposites to 150 ppm of acetone. The response of the Ag/SnO_2/graphene is much higher than that of the SnO_2/graphene. Besides, NO_2 sensing is also observed from the Ag/SnO_2/Graphene ternary nanocomposites at room temperature, in which the response time and recovery time are much shorter than that of SnO_2/Graphene binary nanocomposites [107]. The mechanism is ascribed to the catalysis activity enhancement by Ag nanoparticles which can accelerate the catalysis rate on the surface reactions. During the sensing process, oxygen molecules would react preferentially with Ag nanoparticles forming oxygen anions which transfer to SnO_2 nanoparticles.

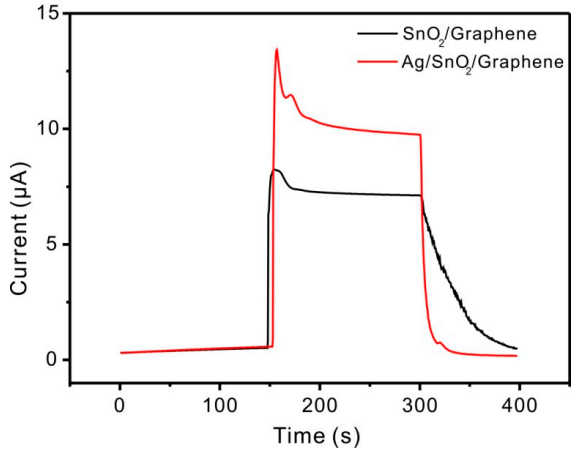

Figure 14. Response comparison between Ag/SnO_2/graphene and SnO_2/graphene nanocomposites to 150 ppm acetone, reproduced with permission from [106]. Copyright Elsevier, 2016.

5. Summary and Perspective

Catalysis plays a significant role for monitoring gas environment by gas sensors. A review on the recent progresses of two representative catalysis-based gas sensors, cataluminescent and

conductometric sensors, is presented. It has been indicated that some great challenges remain for these sensors, including the development of small sized sensing materials to achieve a high reactivity for catalytic reaction, improving the selectivity which show only response to specific target gas, multi-channel signal analysis, weak sensing signals acquirement facing with trace concentration gases, a good long-term stability, and exploring the nature of sensing mechanisms. The cataluminescent gas sensors are summarized from their applications for detecting different gases, while the conductometric ones are introduced on the basis of catalysis effect by noble metal modification and small size.

To meet the increasing requirements on high-performance gas sensors, great efforts are catalysis-related investigations forward. On the one hand, sensitive and selective catalytically sensing nanomaterials are highly desired. Compared to single-component sensing materials, the doped or cooperated composites commonly show an enhanced sensing performance, suggesting that fabricating composites (such as graphene hybrid) would be a promising direction. On the other hand, regarding the detection system, catalysis-based sensor array such as electronic nose, instead of one single sensor, has shown the fascinating advantage of recognizing multi-component gases effectively. Finally, we expect that this review of some details of the typical catalysis-based gas sensors would provide some valuable opportunities for global researchers to develop high-performance sensors, and to explore related surface catalysis chemistries and physics.

Acknowledgments: This work was supported by the State Key Basic Science Program for Nanoscience and Nanotechnology (Grant No. 2013CB934304), and the Natural Science Foundation of China (Grant Nos. 61673367, 21277146, 21177131, 61273066, 11205204 and 61374017).

Conflicts of Interest: The authors declare no conflict of interest.

References

1. Mittal, M.; Kumar, A. Carbon nanotube (CNT) gas sensors for emissions from fossil fuel burning. *Sens. Actuators B Chem.* **2014**, *203*, 349–362. [CrossRef]
2. Zhang, J.; Liu, X.H.; Neri, G.; Pinna, N. Nanostructured materials for room-temperature gas sensors. *Adv. Mater.* **2016**, *28*, 795–831. [CrossRef] [PubMed]
3. Sharma, B.K.; Ahn, J.H. Flexible and stretchable oxide electronics. *Adv. Electron. Mater.* **2016**, *2*. [CrossRef]
4. Dinh, T.V.; Choi, I.Y.; Son, Y.S.; Kim, J.C. A review on non-dispersive infrared gas sensors: Improvement of sensor detection limit and interference correction. *Sens. Actuators B Chem.* **2016**, *231*, 529–538. [CrossRef]
5. Fan, H.Z.; Peng, Z.K.; Yang, H.W.; Zhou, K.W. A new cataluminescence-based gas sensor for simultaneously discriminating benzene and ammonia. *Anal. Methods* **2016**, *8*, 1257–1264. [CrossRef]
6. Wan, X.Y.; Wu, L.Q.; Zhang, L.C.; Song, H.J.; Lv, Y. Novel metal-organic frameworks-based hydrogen sulfide cataluminescence sensors. *Sens. Actuators B Chem.* **2015**, *220*, 614–621. [CrossRef]
7. Griffin, M.J.; Kabir, K.M.M.; Coyle, V.E.; Kandjani, A.E.; Sabri, Y.M.; Ippolito, S.J.; Bhargava, S.K. A nanoengineered conductometric device for accurate analysis of elemental mercury vapor. *Environ. Sci. Technol.* **2016**, *50*, 1384–1392. [CrossRef] [PubMed]
8. Qi, J.; Xu, X.X.; Liu, X.X.; Lau, K.T. Fabrication of textile based conductometric polyaniline gas sensor. *Sens. Actuators B Chem.* **2014**, *202*, 732–740. [CrossRef]
9. Breysse, M.; Claudel, B.; Faure, L.; Guenin, M.; Williams, R.J.J. Chemiluminescense during the catalysis of carbon monoxide oxidation on a thoria surface. *J. Catal.* **1976**, *45*, 137–144. [CrossRef]
10. Rao, Z.M.; Liu, L.J.; Xie, J.Y. Development of a benzene vapour sensor utilizing chemiluminescence on Y_2O_3. *Luminescence* **2008**, *23*, 163–168. [CrossRef] [PubMed]
11. Sha, W.; Ni, S.W.; Zheng, C.H. Development of cataluminescence sensor system for benzene and toluene determination. *Sens. Actuators B Chem.* **2015**, *209*, 297–305. [CrossRef]
12. Men, H.; Chen, D.L.; Zhang, X.T.; Liu, J.J.; Ning, K. Data fusion of electronic nose and electronic tongue for detection of mixed edible-oil. *J. Sens.* **2014**, *2014*. [CrossRef]
13. Liu, C.; Wang, B.Q.; Liu, T.; Sun, P.; Gao, Y.; Liu, F.M.; Lu, GY. Facile synthesis and gas sensing properties of the flower-like NiO-decorated ZnO microstructures. *Sens. Actuators B Chem.* **2016**, *235*, 294–301. [CrossRef]
14. Tang, W.; Wang, J. Enhanced gas sensing mechanisms of metal oxide heterojunction gas sensors. *Acta Phys. Chim. Sin.* **2016**, *32*, 1087–1104.

15. Tang, F.; Guo, C.A.; Chen, J.; Zhang, X.R.; Zhang, S.C.; Wang, X.H. Cataluminescence-based sensors: Principle, instrument and application. *Luminescence* **2015**, *30*, 919–939. [PubMed]
16. Zhang, C.C.; Chen, P.L.; Hu, W.P. Organic field-effect transistor-based gas sensors. *Chem. Soc. Rev.* **2015**, *44*, 2087–2107. [CrossRef] [PubMed]
17. Chatterjee, S.G.; Chatterjee, S.; Ray, A.K.; Chakraborty, A.K. Graphene-metal oxide nanohybrids for toxic gas sensor: A review. *Sens. Actuators B Chem.* **2015**, *221*, 1170–1181. [CrossRef]
18. Llobet, E. Gas sensors using carbon nanomaterials: A review. *Sens. Actuators B Chem.* **2013**, *179*, 32–45. [CrossRef]
19. Mirzaei, A.; Leonardi, S.G.; Neri, G. Detection of hazardous volatile organic compounds (VOCs) by metal oxide nanostructures-based gas sensors: A review. *Ceram. Int.* **2016**, *42*, 15119–15141. [CrossRef]
20. Sanger, A.; Kumar, A.; Kumar, A.; Chandra, R. Highly sensitive and selective hydrogen gas sensor using sputtered grown Pd decorated MnO_2 nanowalls. *Sens. Actuators B Chem.* **2016**, *23*, 8–14. [CrossRef]
21. Alizadeh, T.; Soltani, L.H. Reduced graphene oxide-based gas sensor array for pattern recognition of DMMP vapor. *Sens. Actuators B Chem.* **2016**, *234*, 361–370. [CrossRef]
22. Zhao, L.; Li, X.G.; Wang, J.; Yao, P.J.; Akbar, S.A. Detection of formaldehyde in mixed VOCs gases using sensor array with neural networks. *IEEE Sens. J.* **2016**, *16*, 6081–6086. [CrossRef]
23. Vorobyeva, N.; Rumyantseva, M.; Filatova, D.; Konstantinova, E.; Grishina, D.; Abakumov, A.; Turner, S.; Gaskov, A. Nanocrystalline ZnO(Ga): Paramagnetic centers, surface acidity and gas sensor properties. *Sens. Actuators B Chem.* **2013**, *182*, 555–564. [CrossRef]
24. Manchukutty, S.; Vasa, N.J.; Agarwal, V.; Chandapillai, J. Dual Photoionization source-based differential mobility sensor for trace gas detection in human breath. *IEEE Sens. J.* **2015**, *15*, 4899–4904. [CrossRef]
25. Zhang, H.L.; Zhang, L.C.; Hu, J.; Cai, P.Y.; Lv, Y. A cataluminescence gas sensor based on nanosized V_2O_5 for tert-butyl mercaptan. *Talanta* **2010**, *82*, 733–738. [CrossRef] [PubMed]
26. Yu, L.Z.; Zhang, L.C.; Song, H.J.; Jiang, X.M.; Lv, Y. Hierarchical SnO_2 architectures: Controllable growth on graphene by atmospheric pressure chemical vapour deposition and application in cataluminescence gas sensor. *CrystEngComm* **2014**, *16*, 3331–3340. [CrossRef]
27. Calestani, D.; Mosca, R.; Zanichelli, M.; Villani, M.; Zappettini, A. Aldehyde detection by ZnO tetrapod-based gas sensors. *J. Mater. Chem.* **2011**, *21*, 15532–15536. [CrossRef]
28. Barsan, N.; Weimar, U. Conduction model of metal oxide gas sensors. *J. Electroceram.* **2001**, *7*, 143–167. [CrossRef]
29. Li, Z.H.; Xi, W.; Lu, C. Hydrotalcite-supported gold nanoparticle catalysts as a low temperature cataluminescencesensing platform. *Sens. Actuators B Chem.* **2015**, *219*, 354–360. [CrossRef]
30. Han, J.Y.; Han, F.F.; Ouyang, J.; He, L.X.; Zhang, Y.T.; Na, N. Low temperature CO sensor based on cataluminescence from plasma-assisted catalytic oxidation on Ag doped alkaline-earth nanomaterials. *Nanoscale* **2014**, *6*, 3069–3072. [CrossRef] [PubMed]
31. Shi, G.L.; Sun, B.; Jin, Z.; Liu, J.H.; Li, M.Q. Synthesis of SiO_2/Fe_3O_4 nanomaterial and its application as cataluminescence gas sensor material for ether. *Sens. Actuators B Chem.* **2012**, *171*, 699–704. [CrossRef]
32. Weng, Y.Y.; Zhang, L.C.; Zhu, W.; Lv, Y. One-step facile synthesis of coral-like Zn-doped SnO_2 and its cataluminescence sensing of 2-butanone. *J. Mater. Chem. A* **2015**, *3*, 7132–7138. [CrossRef]
33. Xu, H.L.; Li, Q.Y.; Zhang, L.C.; Zeng, B.R.; Deng, D.Y.; Lv, Y. Transient cataluminescence on flowerlike MgO for discrimination and detection of volatile organic compounds. *Anal. Chem.* **2016**, *88*, 8137–8144. [CrossRef] [PubMed]
34. Tang, J.; Song, H.J.; Zeng, B.R.; Zhang, L.C.; Lv, Y. Cataluminescence gas sensor for ketones based on nanosized $NaYF_4$:Er. *Sens. Actuators B Chem.* **2016**, *222*, 300–306. [CrossRef]
35. Guo, Z.; Jiang, Z.W.; Chen, X.; Sun, B.; Li, M.Q.; Liu, J.H.; Huang, X.J. Novel cocoon-like Au/La_2O_3 nanomaterials: Synthesis and their ultra-enhanced cataluminescence performance to volatile organic compounds. *J. Mater. Chem.* **2011**, *21*, 1874–1879. [CrossRef]
36. Liao, L.; Mai, H.X.; Yuan, Q.; Lu, H.B.; Li, J.C.; Liu, C.; Yan, C.H.; Shen, Z.X.; Yu, T. Single CeO_2 nanowire gas sensor supported with Pt nanocrystals: Gas sensitivity, surface bond states, and chemical mechanism. *J. Phys. Chem. C* **2008**, *112*, 9061–9065. [CrossRef]
37. Guo, W.Y.; Li, J.J.; Tu, Y.F. Studies on the electrochemiluminescent behavior of luminol on indium tin oxide (ITO) glass. *J. Lumin.* **2010**, *130*, 2022–2025. [CrossRef]

38. Yu, L.Z.; Song, H.J.; Tang, Y.R.; Zhang, L.C.; Lv, Y. Controllable deposition of ZnO-doped SnO_2 nanowires on Au/graphene and their application in cataluminescence sensing for alcohols and ketones. *Sens. Actuators B Chem.* **2014**, *203*, 726–735. [CrossRef]
39. Li, B.; Liu, J.F.; Shi, G.L.; Liu, J.H. A research on detection and identification of volatile organic compounds utilizing cataluminescence-based sensor array. *Sens. Actuators B Chem.* **2013**, *177*, 1167–1172. [CrossRef]
40. Hui, J.J.; Li, J.J.; Zhu, Y.; Wei, F.; Zhang, X.R. Nanosized $SrCO_3$-based chemiluminescence sensor for ethanol. *Anal. Chim. Acta* **2002**, *466*, 69–78.
41. Zhang, Z.Y.; Zhang, C.; Zhang, X.R. Development of a chemiluminescence ethanol sensor based on nanosized ZrO_2. *Analyst* **2002**, *127*, 792–796. [CrossRef] [PubMed]
42. Zhang, Z.Y.; Xu, K.; Baeyens, W.R.G.; Zhang, X.R. An energy-transfer cataluminescence reaction on nanosized catalysts and its application to chemical sensors. *Anal. Chim. Acta* **2005**, *535*, 145–152. [CrossRef]
43. Wang, S.M.; Shi, W.Y.; Lu, C. Chemisorbed oxygen on the surface of catalyst-improved cataluminescence selectivity. *Anal. Chem.* **2016**, *88*, 4987–4994. [CrossRef] [PubMed]
44. Zhu, Y.F.; Shi, J.J.; Zhang, Z.Y.; Zhang, C.; Zhang, X.R. Development of a gas sensor utilizing chemiluminescence on nanosized titanium dioxide. *Anal. Chem.* **2002**, *74*, 120–124. [CrossRef] [PubMed]
45. Tang, H.R.; Li, Y.M.; Zheng, C.; Ye, J.; Hou, X.; Lv, Y. An ethanol sensor based on cataluminescence on ZnO nanoparticles. *Talanta* **2007**, *72*, 1593–1597. [CrossRef] [PubMed]
46. Li, B.; Zhang, Y.J.; Liu, J.F.; Xie, X.; Zou, D.; Li, M.Q.; Liu, J.H. Sensitive and selective system of benzene detection based on a cataluminescence sensor. *Luminescence* **2014**, *29*, 332–337. [CrossRef] [PubMed]
47. Zhang, Z.Y.; Zhang, S.C.; Zhang, X.R. Recent development and applications of chemiluminescence sensors. *Anal. Chim. Acta* **2005**, *541*, 37–47. [CrossRef]
48. Song, J.; Huang, K.J.; Wang, N. Gas-sensing properties and in situ diffuse-reflectance Fourier-transform infrared spectroscopy study of diethyl ether adsorption and reactions on SnO_2/rGO film. *J. Mater. Res.* **2016**, *31*, 2035–2045. [CrossRef]
49. Farbod, M.; Joula, M.H.; Vaezi, M. Promoting effect of adding carbon nanotubes on sensing characteristics of ZnO hollow sphere-based gas sensors to detect volatile organic compounds. *Mater. Chem. Phys.* **2016**, *176*, 12–23. [CrossRef]
50. Rad, A.S. Al-doped graphene as modified nanostructure sensor for some ether molecules: Ab-initio study. *Synth. Met.* **2015**, *209*, 419–425. [CrossRef]
51. McCord, P.; Yau, S.L.; Bard, A.J. Chemiluminescence of anodized and etched silicon: Evidence for a luminescent siloxene-like layer on porous silicon. *Science* **1992**, *257*, 68–69. [CrossRef] [PubMed]
52. Wang, Q.H.; Li, B.; Wang, Y.H.; Shou, Z.X.; Shi, G.L. Sensitive and selective cataluminescence-based sensor system for acetone and diethyl ether determination. *Luminescence* **2015**, *30*, 318–324. [CrossRef] [PubMed]
53. Cao, X.A.; Zhang, Z.Y.; Zhang, X.R. A novel gaseous acetaldehyde sensor utilizing cataluminescence on nanosized $BaCO_3$. *Sens. Actuators B Chem.* **2004**, *99*, 30–35. [CrossRef]
54. Yang, P.; Lau, C.; Liang, J.Y.; Lu, J.Z.; Liu, X. Zeolite-based cataluminescence sensor for the selective detection of acetaldehyde. *Luminescence* **2007**, *22*, 473–479. [CrossRef] [PubMed]
55. Zhou, K.W.; Ji, X.L.; Zhang, N.; Zhang, X.R. On-line monitoring of formaldehyde in air by cataluminescence-based gas sensor. *Sens. Actuators B Chem.* **2006**, *119*, 392–397. [CrossRef]
56. Zhang, Z.Y.; Jiang, H.J.; Zhang, X.R. A highly selective chemiluminescent H_2S sensor. *Sens. Actuators B Chem.* **2004**, *102*, 155–161. [CrossRef]
57. Zhou, K.W.; Fan, H.Z.; Gu, C.X.; Liu, B.N. Simultaneous determination of formaldehyde and hydrogen sulfide in air using the cataluminescence of nanosized $Zn_3SnLa_2O_8$. *Microchim. Acta* **2016**, *183*, 1063–1068. [CrossRef]
58. Zeng, B.R.; Zhang, L.C.; Wan, X.Y.; Song, H.J.; Lv, Y. Fabrication of α-Fe_2O_3/g-C_3N_4 composites for cataluminescencesensing of H_2S. *Sens. Actuators B Chem.* **2015**, *211*, 370–376. [CrossRef]
59. Yuliarto, B.; Gumilar, G.; Septiani, N. SnO_2 nanostructure as pollutant gas sensors: Synthesis, sensing performances, and mechanism. *Adv. Mater. Sci. Eng.* **2015**, *2015*, 694823. [CrossRef]
60. Sutka, A.; Gross, K.A. Spinel ferrite oxide semiconductor gas sensors. *Sens. Actuators B Chem.* **2016**, *222*, 95–105. [CrossRef]
61. Kim, J.H.; Jeong, H.M.; Na, C.W.; Yoon, J.W.; Abdel-Hady, F.; Wazzan, A.A.; Lee, J.H. Highly selective and sensitive xylene sensors using Cr_2O_3-$ZnCr_2O_4$ hetero-nanostructures prepared by galvanic replacement. *Sens. Actuators B Chem.* **2016**, *235*, 498–506. [CrossRef]

62. Mirzaei, A.; Hashemi, B.; Janghorban, K. alpha-Fe_2O_3 based nanomaterials as gas sensors. *J. Mater. Sci. Mater. Electron.* **2016**, *27*, 3109–3144. [CrossRef]
63. Huang, X.J.; Wang, L.C.; Sun, Y.F.; Meng, F.L.; Liu, J.H. Quantitative analysis of pesticide residue based on the dynamic response of a single SnO_2 gas sensor. *Sens. Actuators B Chem.* **2004**, *99*, 330–335. [CrossRef]
64. Sun, Y.F.; Huang, X.J.; Meng, F.L.; Liu, J.H. Study of influencing factors of dynamic measurements based on SnO_2 gas sensor. *Sensors* **2004**, *4*, 95–104. [CrossRef]
65. Meng, F.L.; Li, M.Q.; Chen, Y.; Jia, Y.; Liu, J.Y.; Huang, J.R.; Liu, J.H. Dynamic prebreakdown current measurement of nanotips-based gas ionization sensor application at ambient atmosphere. *IEEE Sens. J.* **2009**, *9*, 435–440. [CrossRef]
66. Sun, Y.F.; Liu, S.B.; Meng, F.L.; Liu, J.Y.; Jin, Z.; Kong, L.T.; Liu, J.H. Metal oxide nanostructures and their gas sensing properties: A review. *Sensors* **2012**, *12*, 2610–2631. [CrossRef] [PubMed]
67. San, X.G.; Wang, G.S.; Liang, B.; Song, Y.M.; Gao, S.Y.; Zhang, J.S.; Meng, F.L. Catalyst-free growth of one-dimensional ZnO nanostructures on SiO_2 substrate and in situ investigation of their H_2 sensing properties. *J. Alloy Compd.* **2015**, *622*, 73–78. [CrossRef]
68. Wu, H.; Xu, C.; Xu, J.; Lu, L.F.; Fan, Z.Y.; Chen, X.Y.; Song, Y.; Li, D.D. Enhanced supercapacitance in anodic TiO_2 nanotube films by hydrogen plasma treatment. *Nanotechnology* **2013**, *24*, 455401. [CrossRef] [PubMed]
69. Wu, H.; Li, D.D.; Zhu, X.F.; Yang, C.Y.; Liu, D.F.; Chen, X.Y.; Song, Y.; Lu, L.F. High-performance and renewable supercapacitors based on TiO_2 nanotube array electrodes treated by an electrochemical doping approach. *Electrochim. Acta* **2014**, *116*, 129–136. [CrossRef]
70. Meng, F.L.; Zhang, L.; Jia, Y.; Liu, J.Y.; Sun, Y.F.; Luo, T.; Li, M.Q.; Liu, J.H.; Huang, X.J. Electronic chip based on self-oriented carbon nanotube microelectrode array to enhance the sensitivity of indoor air pollutants capacitive detection. *Sens. Actuators B Chem.* **2011**, *153*, 103–109. [CrossRef]
71. Biswal, R.C. Pure and Pt-loaded gamma iron oxide as sensor for detection of sub ppm level of acetone. *Sens. Actuators B Chem.* **2011**, *157*, 183–188. [CrossRef]
72. Banerjee, N.; Bhowmik, B.; Roy, S.; Sarkar, C.K.; Bhattacharyya, P. Anomalous recovery characteristics of Pd modified ZnO nanorod based acetone sensor. *J. Nanosci. Nanotechnol.* **2013**, *13*, 6826–6834. [CrossRef] [PubMed]
73. Wang, X.J.; Wang, W.; Liu, Y.L. Enhanced acetone sensing performance of Au nanoparticles functionalized flower-like ZnO. *Sens. Actuators B Chem.* **2012**, *168*, 39–45. [CrossRef]
74. Yin, M.L.; Liu, M.D.; Liu, S.Z. Diameter regulated ZnO nanorod synthesis and its application in gas sensor optimization. *J. Alloy Compd.* **2014**, *586*, 436–440. [CrossRef]
75. Song, H.Y.; Yang, H.; Ma, X.C. A comparative study of porous ZnO nanostructures synthesized from different zinc salts as gas sensor materials. *J. Alloy Compd.* **2013**, *578*, 272–278. [CrossRef]
76. Wang, L.W.; Wang, S.R.; Xu, M.J.; Hu, X.J.; Zhang, H.X.; Wang, Y.S.; Huang, W.P. A Au-functionalized ZnO nanowire gas sensor for detection of benzene and toluene. *Phys. Chem. Chem. Phys.* **2013**, *15*, 17179–17186. [CrossRef] [PubMed]
77. Gu, C.P.; Li, S.S.; Huang, J.R.; Shi, C.C.; Liu, J.H. Preferential growth of long ZnO nanowires and its application in gas sensor. *Sens. Actuators B Chem.* **2013**, *177*, 453–459. [CrossRef]
78. Yeo, J.; Hong, S.; Wanit, M.; Kang, H.W.; Lee, D.; Grigoropoulos, C.P.; Sung, H.J.; Ko, S.H. Rapid, one-step, digital selective growth of ZnO nanowires on 3D structures using laser induced hydrothermal growth. *Adv. Funct. Mater.* **2013**, *23*, 3316–3323. [CrossRef]
79. Lim, Y.T.; Son, J.Y.; Rhee, J.S. Vertical ZnO nanorod array as an effective hydrogen gas sensor. *Ceram. Int.* **2013**, *39*, 887–890. [CrossRef]
80. Ghosh, M.; Karmakar, D.; Basu, S.; Jha, S.N.; Bhattacharyya, D.; Gadkari, S.C.; Gupta, S.K. Effect of size and aspect ratio on structural parameters and evidence of shape transition in zinc oxide nanostructures. *J. Phys. Chem. Solids* **2014**, *75*, 543–549. [CrossRef]
81. Zhang, S.L.; Lim, J.O.; Huh, J.S.; Noh, J.S.; Lee, W. Two-step fabrication of ZnO nanosheets for high-performance VOCs gas sensor. *Curr. Appl. Phys.* **2013**, *13* (Suppl. 2), S156–S161. [CrossRef]
82. Xiang, D.; Qu, F.Y.; Chen, X.; Yu, Z.; Cui, L.R.; Zhang, X.; Jiang, J.J.; Lin, H.M. Synthesis of porous ZnO nanospheres for gas sensor and photocatalysis. *J. Sol-Gel Sci. Technol.* **2014**, *69*, 370–377. [CrossRef]
83. Meng, F.L.; Hou, N.N.; Jin, Z.; Sun, B.; Guo, Z.; Kong, L.T.; Xiao, X.H.; Wu, H.; Li, M.Q.; Liu, J.H. Ag-decorated ultra-thin porous single-crystalline ZnO nanosheets prepared by sunlight induced solvent reduction and their highly sensitive detection of ethanol. *Sens. Actuators B Chem.* **2015**, *209*, 975–982. [CrossRef]

84. Sun, Y.F.; Ge, S.; Huang, H.H.; Zheng, H.X.; Jin, Z.; Shan, J.H.; Gu, C.P.; Huang, X.J.; Meng, F.L. Novel volatile organic compound (VOC) sensor based on Ag-decorated porous single-crystalline ZnO nanosheets. *Mater. Express* **2016**, *6*, 191–197. [CrossRef]
85. Gu, C.P.; Huang, H.H.; Huang, J.R.; Jin, Z.; Zheng, H.X.; Liu, N.; Li, M.Q.; Liu, J.H.; Meng, L.M. Chlorobenzene sensor based on Pt-decorated poroussingle-crystalline ZnO nanosheets. *Sens. Actuators A Phys.* **2016**, *252*, 96–103. [CrossRef]
86. Qin, Y.X.; Fan, G.T.; Liu, K.X.; Hu, M. Vanadium pentoxide hierarchical structure networks for high performance ethanol gas sensor with dual working temperature characteristic. *Sens. Actuators B Chem.* **2014**, *190*, 141–148. [CrossRef]
87. Hou, N.N.; Jin, Z.; Sun, B.; Sun, Y.F.; Shen, W.; Guo, Z.; Kong, L.T.; Li, M.Q.; Meng, F.L. New strategy for rapid detection of the simulants of persistent organic pollutants using gas sensor based on 3D porous single-crystalline ZnO nanosheets. *IEEE Sens. J.* **2015**, *15*, 3668–3674. [CrossRef]
88. Meng, D.; Wang, G.S.; San, X.G.; Song, Y.M.; Shen, Y.B.; Zhang, Y.J.; Wang, K.J.; Meng, F.L. Synthesis of WO_3 flower-like hierarchical architectures and their sensing properties. *J. Alloy Compd.* **2015**, *649*, 731–738. [CrossRef]
89. Alenezi, M.R.; Henley, S.J.; Emerson, N.G.; Silva, S.R.P. From 1D and 2D ZnO nanostructures to 3D hierarchical structures with enhanced gas sensing properties. *Nanoscale* **2014**, *6*, 235–247. [CrossRef] [PubMed]
90. Meng, F.; Ge, S.; Jia, Y.; Sun, B.; Sun, Y.; Wang, C.; Wu, H.; Jin, Z.; Li, M. Interlaced nanoflake-assembled flower-like hierarchical ZnO microspheres prepared by bisolvents and their sensing properties to ethanol. *J. Alloy Compd.* **2015**, *632*, 645–650. [CrossRef]
91. Meng, F.L.; Hou, N.N.; Ge, S.; Sun, B.; Jin, Z.; Shen, W.; Kong, L.T.; Guo, Z.; Sun, Y.F.; Wu, H.; et al. Flower-like hierarchical structures consisting of porous single-crystalline ZnO nanosheets and their gas sensing properties to volatile organic compounds (VOCs). *J. Alloy Compd.* **2015**, *626*, 124–130. [CrossRef]
92. Meng, F.L.; Hou, N.N.; Jin, Z.; Sun, B.; Li, W.Q.; Xiao, X.H.; Wang, C.; Li, M.Q.; Liu, J.H. Sub-ppb detection of acetone using Au-modified flower-like hierarchical ZnO structures. *Sens. Actuators B Chem.* **2015**, *219*, 209–217. [CrossRef]
93. Lai, H.Y.; Chen, C.H. Highly sensitive room-temperature CO gas sensors: Pt and Pd nanoparticle-decorated In_2O_3 flower-like nanobundles. *J. Mater. Chem.* **2012**, *22*, 13204–13208. [CrossRef]
94. Liu, C.; Kuang, Q.; Xie, Z.X.; Zheng, L.S. The effect of noble metal (Au, Pd and Pt) nanoparticles on the gas sensing performance of SnO_2-based sensors: A case study on the {221} high-index faceted SnO_2 octahedra. *CrystEngComm* **2015**, *17*, 6308–6313. [CrossRef]
95. Jeon, J.M.; Shim, Y.S.; Han, S.D.; Kim, D.H.; Kim, Y.H.; Kang, C.Y.; Kim, J.S.; Kim, M.Y.; Jang, H.W. Vertically ordered SnO_2 nanobamboos for substantially improved detection of volatile reducing gases. *J. Mater. Chem. A* **2015**, *3*, 17939–17945. [CrossRef]
96. Shim, Y.S.; Kim, D.H.; Jeong, H.Y.; Kim, Y.H.; Nahm, S.H.; Kang, C.Y.; Kim, J.S.; Lee, W.Y.; Jang, H.W. Utilization of both-side metal decoration in close-packed SnO_2 nanodome arrays for ultrasensitive gas sensing. *Sens. Actuators B Chem.* **2015**, *213*, 314–321. [CrossRef]
97. Shim, Y.S.; Moon, H.G.; Kim, D.H.; Zhang, L.H.; Yoon, S.J.; Yoon, Y.S.; Kang, C.Y.; Jang, H.W. Au-decorated WO_3 cross-linked nanodomes for ultrahigh sensitive and selective sensing of NO_2 and C_2H_5OH. *RSC Adv.* **2013**, *3*, 10452–10459. [CrossRef]
98. Shim, Y.S.; Zhang, L.H.; Kim, D.H.; Kim, Y.H.; Choi, Y.R.; Nahm, S.H.; Kang, C.Y.; Lee, W.Y.; Jang, H.W. Highly sensitive and selective H_2 and NO_2 gas sensors based on surface-decorated WO_3 nanoigloos. *Sens. Actuators B Chem.* **2014**, *198*, 294–301. [CrossRef]
99. Xu, C.N.; Tamaki, J.; Miura, N.; Yamazoe, N. Grain-size effects on gas sensitivity of porous SnO_2-based elements. *Sens. Actuators B Chem.* **1991**, *3*, 147–155. [CrossRef]
100. Meng, F.L.; Li, H.H.; Kong, L.T.; Liu, J.Y.; Jin, Z.; Li, W.; Jia, Y.; Liu, J.H.; Huang, X.J. Parts per billion-level detection of benzene using SnO_2/graphene nanocomposite composed of sub-6 nm SnO_2 nanoparticles. *Anal. Chim. Acta* **2012**, *736*, 100–107. [CrossRef] [PubMed]
101. Mansha, M.; Qurashi, A.; Ullah, N.; Bakare, F.O.; Khan, I.; Yamani, Z.H. Synthesis of In_2O_3/graphene heterostructure and their hydrogen gas sensing properties. *Ceram. Int.* **2016**, *42*, 11490–11495. [CrossRef]

102. Liu, J.Y.; Guo, Z.; Meng, F.L.; Jia, Y.; Liu, J.H. A novel antimony-carbon nanotube-tin oxide thin film: Carbon nanotubes as growth guider and energy buffer. Application for indoor air pollutants gas sensor. *J. Phys. Chem. C* **2008**, *112*, 6119–6125. [CrossRef]
103. Meng, F.L.; Jia, Y.; Liu, J.Y.; Li, M.Q.; Sun, Y.F.; Liu, J.H.; Huang, X.J. Nanocomposites of sub-10 nm SnO_2 nanoparticles and MWCNTs for detection of aldrin and DDT. *Anal. Methods* **2010**, *2*, 1710–1714. [CrossRef]
104. Srivastava, V.; Jain, K. At room temperature graphene/SnO_2 is better than MWCNT/SnO_2 as NO_2 gas sensor. *Mater. Lett.* **2016**, *169*, 28–32. [CrossRef]
105. Meng, F.L.; Guo, Z.; Huang, X.J. Graphene-based hybrids for chemiresistive gas sensors. *TrAC Trend Anal. Chem.* **2015**, *68*, 37–47. [CrossRef]
106. Ge, S.; Zheng, H.X.; Sun, Y.F.; Jin, Z.; Shan, J.H.; Wang, C.; Wu, H.; Li, M.Q.; Meng, F.L. Ag/SnO_2/graphene ternary nanocomposites and their sensing properties to volatile organic compounds. *J. Alloy Compd.* **2016**, *659*, 127–131. [CrossRef]
107. Wang, Z.Y.; Zhang, Y.; Liu, S.; Zhang, T. Preparation of Ag nanoparticles-SnO_2 nanoparticles-reduced graphene oxide hybrids and their application for detection of NO_2 at room temperature. *Sens. Actuators B Chem.* **2016**, *222*, 893–903. [CrossRef]